

# Nanoscale

Accepted Manuscript



This is an *Accepted Manuscript*, which has been through the Royal Society of Chemistry peer review process and has been accepted for publication.

*Accepted Manuscripts* are published online shortly after acceptance, before technical editing, formatting and proof reading. Using this free service, authors can make their results available to the community, in citable form, before we publish the edited article. We will replace this *Accepted Manuscript* with the edited and formatted *Advance Article* as soon as it is available.

You can find more information about *Accepted Manuscripts* in the [Information for Authors](#).

Please note that technical editing may introduce minor changes to the text and/or graphics, which may alter content. The journal's standard [Terms & Conditions](#) and the [Ethical guidelines](#) still apply. In no event shall the Royal Society of Chemistry be held responsible for any errors or omissions in this *Accepted Manuscript* or any consequences arising from the use of any information it contains.



## Light-controllable dispersion and recovery of graphenes and carbon nanotubes using a photo-switchable surfactant

Received 00th January 20xx,  
Accepted 00th January 20xx

Thomas M. McCoy,<sup>a</sup> Amelia C. Y. Liu<sup>b</sup> and Rico F. Tabor\*<sup>a</sup>

DOI: 10.1039/x0xx00000x

www.rsc.org/

**The aqueous dispersibility of carbon-based nanomaterials, namely graphene oxide (GO), reduced graphene oxide (rGO) and carbon nanotubes (CNTs), can be controlled by light via the photoisomerisation of a photoswitchable surfactant molecule adsorbed to the surface of these materials. By incorporating a cationic azobenzene photosurfactant into these systems, GO, rGO and CNT dispersions can be separated and redispersed on command utilising UV radiation at 365 nm, whereby the surfactant molecules change from the *trans* to the *cis* isomer. This increases their aqueous solubility and in turn, alters their adsorption affinity for the GO and rGO sheets such that the ratio of free to adsorbed surfactant molecules changes significantly, allowing for reversible phase separation of the colloids. These effects present a unique method for controlling the dispersion behaviour of two-dimensional nanomaterials using light as a clean and low energy external stimulus.**

### Introduction

Graphene and related carbon nanomaterials (CNMs) show exceptional potential in a vast number of technological applications, stemming from their leading conductive and mechanical properties.<sup>1</sup> However, the largely hydrophobic nature of graphene causes it to be colloiddally unstable in water without the aid of surfactant stabilisers,<sup>2</sup> and hence processing and deploying it in aqueous systems remains challenging. Conversely, graphene oxide (GO) and reduced graphene oxide (rGO) sheets present hydrophilic functional groups and bear large negative surface potentials in water,<sup>3,4</sup> causing them to disperse readily, and making their use in aqueous systems viable. This important feature, along with the enormous surface area of GO/rGO sheets have paved the way for the use of these materials as excellent stabilisers of oil-water interfaces,<sup>5,6</sup> as well as promising adsorbents for the treatment of wastewater.<sup>7</sup>

To enable the scale-up in both synthesis and use of CNMs, effective methods for their dispersion and recovery from aqueous systems must be developed. Many GO and rGO composites have been developed with stimulus-responsive properties that facilitate this process, with a particular focus on magnetic recovery.<sup>8</sup> Magnetic GO/rGO composites have been formulated for the purpose of environmental decontamination,<sup>9</sup> although the vast majority focus on covalent tethering of magnetic particles, limiting the uses of the recovered CNM. Despite this, the use of external stimuli to control CNM dispersion is particularly appealing, and of the possible stimuli, light is perhaps the 'cleanest'.

In other soft systems and dispersions, photoswitchable stabilisers have been used to great effect to control stability and cause phase separations that enable recovery of materials from DNA to metal nanoparticles.<sup>10,11</sup> Molecular switches that change their structural configuration – and hence properties – when exposed to light of a specific wavelength are of great interest for the development of light-tunable devices and photo-modulation of dispersion stability.<sup>12,13</sup> The cationic surfactant butylphenyl-4-diazeno-4-butoxyphenyl-trimethylammonium bromide (azoTAB) contains the widely-used azobenzene chromophore, known for its *trans*–*cis* photoisomerisation when exposed to UV light at *ca* 350 nm (Fig. 1g).<sup>14–16</sup> In this process, the C=N=N–C dihedral angle changes from 180° to around 11°,<sup>17</sup> and the  $\pi \rightarrow \pi^*$  absorption band becomes dramatically lower in intensity (Fig. 1h). With this altered structure comes a significant increase in dipole moment (typically from *ca* 0.4 to 3.5 D) that serves to increase the aqueous solubility of the surfactant.<sup>18</sup>

Here, we utilise a simple photoswitchable surfactant (azoTAB – chemical and photochemical characterization provided in Supplementary Information) to reversibly control the stability of carbon nanomaterials, specifically demonstrating the effect for GO, rGO and CNTs (Fig. 1a–f). By exploring the molecular basis for adsorption and stabilisation/flocculation effects, we are able to unravel the complex interplay of charge,  $\pi$ -stacking and hydrophobic interactions that determine stability in these systems. These systems provide new horizons for the deployment and capture of carbon nanomaterials in aqueous environments, providing reversible separations at low materials and energy cost.

<sup>a</sup>School of Chemistry, Monash University, Clayton, VIC 3800, Australia

<sup>b</sup>Monash Centre for Electron Microscopy and School of Physics and Astronomy, Monash University, Clayton, VIC 3800, Australia

† Electronic Supplementary Information (ESI) available: Includes further details on materials characterization, photo response, adsorption and SANS analysis. See DOI: 10.1039/x0xx00000x

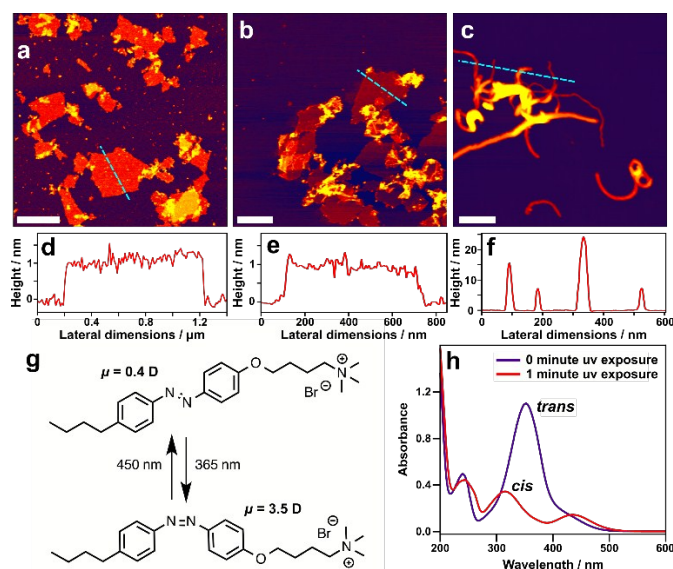


Fig. 1: (a, b & c) AFM height images of GO (a), rGO (b) and CNTs (c) dried onto mica. The dashed lines correspond to the height profiles in d, e and f and the scale bars represent 1  $\mu\text{m}$ , 500 nm and 200 nm respectively. (g) Structural schematic showing the reversible, photo-induced *trans*  $\rightarrow$  *cis* isomerisation of azoTAB. (h) UV-visible spectra of *trans*- and *cis*-azoTAB.

## Results and Discussion

### Reduced graphene oxide

The dispersibility of CNMs is intimately related to their dimensions, charge and hydrophobicity,<sup>4,19</sup> and here we start by investigating the photo-induced phase separation of rGO, the most 'graphene like' of the materials explored. When GO is chemically or physically reduced to rGO, its innate hydrophobicity increases due to the loss of hydrophilic functional groups, and rGO is therefore generally only metastable in aqueous conditions.<sup>3,20,21</sup> When adding a cationic surfactant that would be expected to adsorb readily to the negative charge sites on rGO<sup>22</sup> thereby reducing its effective surface potential and increasing its hydrophobicity, it is thus unsurprising that the dispersion fully flocculates, even at very low concentrations of azoTAB in both *trans*- and *cis*-dominated isomerisation states (Fig. 2a and b). By only modest changes in concentration, essentially full dispersion or flocculation can be achieved (Fig. 2c).

It is important to note here that azobenzene molecules do not exclusively exist in one isomeric state, but instead equilibrate to a statistical photostationary state comprising a proportion of both isomers, which varies depending on the illumination conditions.<sup>23-26</sup> Upon irradiation with UV light, the proportion of *cis* configured molecules increases; for the surfactant chemistry used in these experiments, the *cis* isomer proportion has been shown previously<sup>27,28</sup> to be 25% in the *trans*-dominated photostationary state that exists in ambient lighting conditions, and 95% in the *cis*-dominated photostationary state that exists after equilibration under UV light at 365 nm (assessed by UV-visible spectrophotometric measurements here, see Supplementary Information). For the sake of brevity henceforth we use the terms *trans* and *cis* to refer to the *trans*-dominated and *cis*-dominated states respectively.

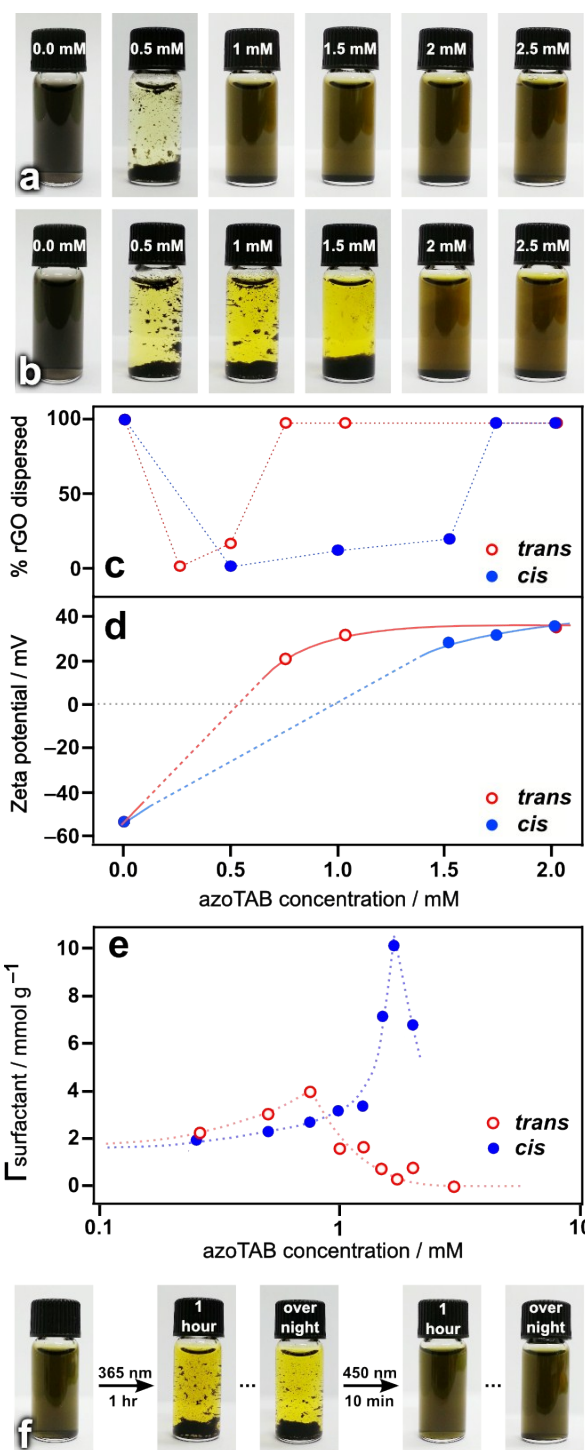


Fig. 2: (a) Samples containing 0.1 mg/mL rGO and the specified concentrations of azoTAB, 30 minutes after preparation. (b) Identical samples in which the azoTAB solution was irradiated at 365 nm for 10 minutes before the rGO was added. (c) Quantification of the % of rGO dispersed for various concentrations of azoTAB, obtained spectrophotometrically. (d) Phase analysis light scattering data of rGO for increasing azoTAB concentrations. Measurements could not be conducted in the dashed regions as the rGO dispersion was unstable here. (e) Adsorption isotherm of azoTAB in *trans* and *cis* dominated states onto rGO. All samples are at pH 11. (f) An image series of the same 0.1 mg/mL rGO dispersion, demonstrating the effects of photoisomeration of the surfactant (1.2 mM).

As surfactant concentration is increased to the CMC of azoTAB (1 mM in the *trans* state and 2 mM in the *cis* state, see Supplementary Information) and beyond, the rGO remains fully dispersed. It can also be observed quantitatively in the azoTAB/rGO adsorption isotherm (Fig. 2e) that azoTAB adsorption drops off significantly at and past these concentrations. This unexpected result indicates that steric stabilisation by further surfactant adsorption is unlikely to be the effect causing stability of the rGO dispersions at high surfactant loadings. Instead, the highly positive zeta potentials (>30 mV) obtained (Fig. 2d) indicate re-stabilisation by charging of the colloids, presumably *via* surfactant adsorption through  $\pi$ -stacking interactions. It has been noted in previous molecular modelling studies that for small aromatics adsorbing to carbon nanotubes,  $\pi$ -stacking interactions are “the most important ingredient” in adsorption,<sup>29</sup> and substituents play only a minor role.<sup>30</sup> This would indicate that the aromatic core of the azoTAB surfactant used here would experience favourable interactions with the aromatic regions of the CNMs. The reduction in adsorbed amount is curious, and may reflect a reconfiguration of the partitioning within the system when moving to a 3-state equilibrium (adsorbed, monomeric and micellised surfactant).

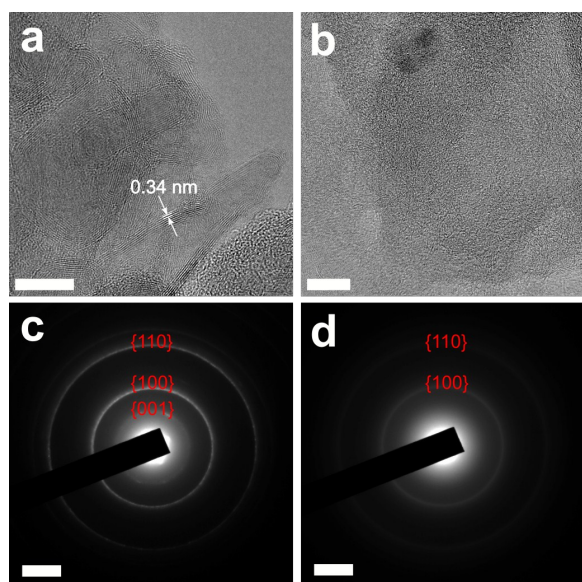


Fig. 3: (a & b) High-resolution TEM images of rGO aggregates prepared from aqueous samples without (a) and with azoTAB present (b). The scale bars represent 10 nm. For the rGO only sample, the arrows indicate the apparent spacing between sheets, which is on average 0.34 nm. The corresponding selected area electron diffraction (SAED) patterns (c & d) are shown below the images to which they correspond. The scale bars represent  $3 \text{ nm}^{-1}$ , and the numbers are the Miller indices for the interplanar and in-plane spacings.

The difference in surfactant concentration of the two isomers required to induce flocculation of the rGO provides an accessible window in which the dispersibility of the material can be reversibly controlled by exploiting the photo-induced switch of the azobenzene group. By choosing a concentration between 1 and 2 mM (e.g. 1.2 mM), it can be seen that it is possible to reversibly flocculate and redisperse the rGO by using light (Fig. 2f). It is noteworthy that significantly longer illumination times were

required to destabilise the colloid when the rGO was present compared to Figure 2b, where the surfactant solutions were irradiated before the rGO was added, due to added optical density of the rGO dispersion. Irradiation with blue light (*ca* 450 nm) then served to restabilise the rGO, and although not required, this process could be accelerated by short bursts of ultrasonication. The retained stability of the dispersion after being left overnight shows that the restabilisation is a direct result of the isomerisation state of the surfactant.

To further characterise the morphology and aggregation of the carbon nanomaterials, we performed high-resolution transmission electron microscopy (HR-TEM) of two samples: rGO (Fig. 3a) and rGO with azoTAB (Fig. 3b). Upon drying the samples for TEM, the materials are observed in both cases as large aggregates or clumps at low magnification (see Supplementary Information), which is unsurprising given the hydrophobic nature of rGO. However, by observing these aggregates at high resolution (Figs. 3a and b), there are noticeable differences in the structure of the aggregates that are formed. When azoTAB is not present, the rGO sheets aggregate and form curved stacks, indicating the presence and alignment of graphitic regions, but also highlighting the presence of defects in the layers. The average interlayer spacing of these stacks is 0.34 nm, which is consistent with previous findings.<sup>31,32</sup> When azoTAB is present however, the sheets do not stack. This suggests that adsorbed surfactant molecules disrupt the strong  $\pi$ -stacking interactions that occur between the naked rGO sheets, pointing to a disordered fractal-type aggregation (as confirmed by small-angle neutron scattering measurements below). These differences indicate the significance of surfactant adsorption, and are reinforced by the corresponding selected area electron diffraction (SAED) patterns (Figs. 3c and d). There is a much higher degree of paracrystalline order in the rGO sample with no surfactant, as indicated by the sharp rings in the diffraction pattern (Fig. 3c). These rings correspond to the interplanar spacing of  $0.34 \pm 0.02 \text{ nm}$  and the in-plane spacings of  $0.21 \pm 0.02 \text{ nm}$  and  $0.12 \pm 0.02 \text{ nm}$ . The SAED pattern from the rGO/azoTAB sample (Fig. 3d) shows significantly more diffuse rings, with only the in-plane spacings present, reaffirming the absence of stacked sheets. Further information on sample preparation and image analysis can be found in the Supplementary Information.

### Carbon nanotubes

It is seen that another hydrophobic CNM in the form of carbon nanotubes (CNTs) could be dispersed and recovered using the same method as for rGO above. CNTs do not typically disperse in water, but have been found to do so with the aid of surfactant molecules and sonication.<sup>33</sup> In the case of azoTAB, the CNTs are found to disperse well when the surfactant is in the more surface active *trans* configuration, with dispersions achieved at sub-CMC concentrations (0.5 mM), whereas it can be seen that the *cis* isomer does not effectively disperse the CNTs at concentrations below 1.5 mM and they settle out after only 1 hour (Fig. 4a). When using azoTAB as a dispersant for CNTs, dispersion was incomplete, with few systems achieving greater than 50% dispersion (Fig. 4b), however these results could be significantly improved with longer sonication times and the experiments performed here were intended to distinguish the effects of the *trans* versus *cis* configuration. In addition, the highly polydisperse nature of the multiwalled CNTs used here meant that the separation was not as ‘clean’ (*i.e.* complete) as for rGO, and therefore further studies were not performed.

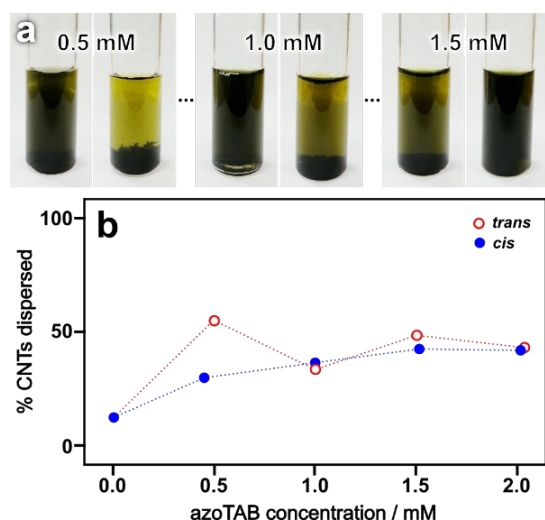


Fig. 4: (a) Samples containing 0.05 mg/mL of CNTs and azoTAB in *trans*-dominated (left) and *cis*-dominated (right) states. These samples were sonicated for approximately 2 minutes and images were taken after 1 hour. (b) Quantification of the % of CNTs dispersed for various concentrations of azoTAB, obtained spectrophotometrically.

### Graphene oxide

It is unsurprising that on moving to graphene oxide, a hydrophilic and water-dispersible CNM, that very different behaviour is seen. Here, the dispersion stability is innately much higher and it is therefore more challenging to effect destabilisation through surfactant adsorption. Although significant adsorption was seen in the isotherm when mixing GO with azoTAB at pH 3 (Fig. 5c), at the surfactant concentrations where rGO flocculated, GO is instead stable. Notably, a significant difference can be observed in the level of adsorption between not only the *trans* and *cis* forms of azoTAB, but also when the photosurfactant solution is irradiated pre-adsorption GO when compared to UV irradiation of the already-adsorbed *trans* dominated azoTAB. This result is in line with expectation from the larger dipole moment and increased solubility of the *cis* isomer, which would cause a shift in the dynamic equilibrium of the system such that the surfactant partitions more into the bulk solution. The difference in adsorption from isomerisation pre- versus post-adsorption could indicate that adsorption of the surfactant to the GO in the *trans* form means that molecules are somewhat stabilised towards desorption.

When examining the same systems in basic conditions (pH 10), it was found that higher concentrations of azoTAB (> 0.3 mM) were required to flocculate the GO (Fig. 5a,b). It can also be seen that flocculation occurred less readily when the surfactant was in the *cis* state (Fig. 5b), reinforcing the notion that light can be used to control the aggregation state of these systems. Surprisingly, when the same isotherm was determined at pH 10 (Fig. 5c, hollow symbols) there was no significant change in the adsorbed amount of surfactant, suggesting that adsorption is not driven solely by electrostatics. As discussed previously, this is likely due to favourable  $\pi$ -stacking interactions between the azobenzene core and aromatic regions of the GO sheets, indicated by previous density functional theory (DFT) studies on carbon nanotubes.<sup>29,30</sup> Investigation of the surface charge on the GO sheets showed that increasing the concentration of azoTAB resulted in a gradual

increase in the zeta potential of the system (Fig. 5d). This accounts for the destabilisation of the dispersion due to insufficient electrical double-layer interactions between sheets. However, given that the zeta potential of the GO increases only marginally with added azoTAB, it is clear that charge-based interactions are not the predominant mode of adsorption in these systems, and that the interactions due to  $\pi$ -stacking<sup>29,30</sup> and potentially hydrophobicity are more significant. The important role of hydrophobic interactions between the tail-group and carbon nanomaterial in adsorption of surfactants onto CNMs has been indicated previously;<sup>34</sup> combined with the capacity for strong  $\pi$ -stacking interactions, it therefore becomes clear that in this case, it is likely that tail-group chemistry is more significant than the surfactant head-group in determining the level and mode of surfactant adsorption.

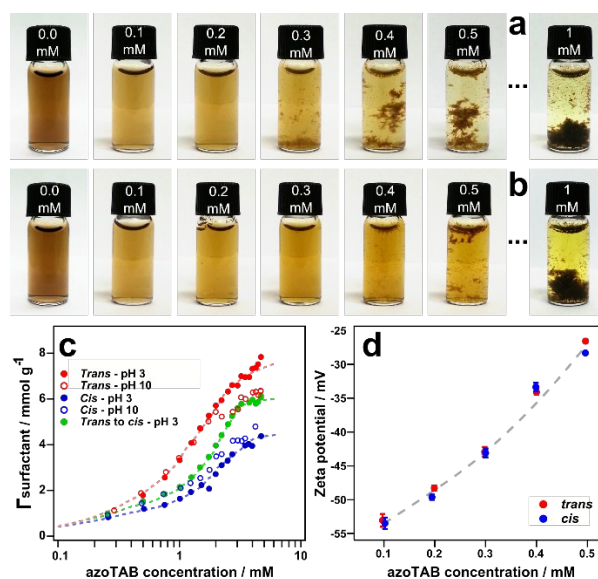


Fig. 5: (a) Samples comprising 0.2 mg/mL GO and the specified concentrations of azoTAB 30 mins (0–0.5 mM) or 12 h (1 mM) after preparation. (b) Identical samples in which the azoTAB was irradiated at 365 nm for 10 minutes before the GO was added. All samples are at approximately pH 10. (c) Adsorption isotherm of azoTAB photosurfactant onto GO at high (open symbols) and low (solid symbols) pH. The green data series corresponds to samples that were irradiated with UV light for 10 minutes after GO was incorporated into the system. (d) Phase analysis light scattering data showing the change in zeta potential of GO for increasing concentrations of azoTAB in the *trans* and *cis* state. The dashed line is a guide to the eye.

### SANS analysis

To further explore the aggregation mechanism and morphology induced by interaction of azoTAB with GO and rGO, small-angle neutron scattering (SANS) was employed, whereby the effects of surfactant concentration and irradiation on assembly were analysed. The scattering seen (Fig. 6a–c) is characteristic of fractal aggregation, where intensity increases rapidly at low scattering vector  $q$  (an inverse length scale), indicating the formation of large structures with poorly defined morphology; thus a mass fractal model was used to fit these data. It can be seen that scattering intensity is greater for GO than rGO systems, and also greater for

*trans* than *cis* (Fig. 6a–c). Given the previous results of the isotherms this is not surprising, as the surfactant molecules were found to have a higher affinity for GO than rGO, and are responsible for the majority of the scattered intensity due to their greater contrast than the CNMs (see Supplementary Information).

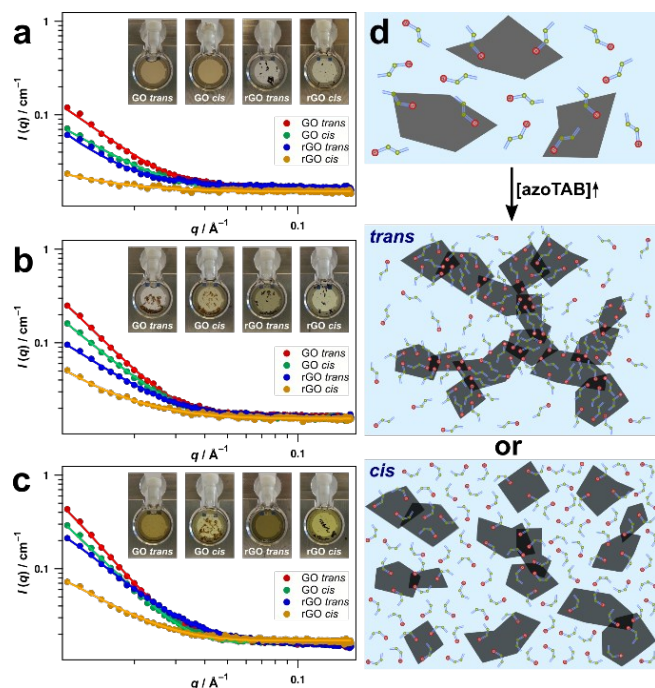


Fig. 6: Small-angle neutron scattering data of GO (0.15 mg/mL) or rGO (0.1 mg/mL) in 0.25 mM (a), 0.5 mM (b) and 1 mM (c) solutions of azoTAB. Symbols represent the experimental SANS data and solid lines are the corresponding theoretical fits. The insets are images of each measured sample in 2 mm path-length quartz cells. (d) A schematic showing the proposed formation of fractal aggregates as surfactant loadings are increased in the *trans* and *cis* state. For simplicity, surfactant molecules are displayed in only one isomeric state rather than the respective photostationary states.

By exploring systems where the photosurfactant concentration is changed as well as its isomerisation state (Fig. 6a–c), it becomes clear that the level of surfactant adsorption is the key process driving flocculation in these systems (Fig. 6d). Differences in the fitting parameters from the mass fractal model used to quantify these data<sup>35</sup> indicate that the spatially inhomogeneous flocs become more compacted with increased surfactant loading. Fractal aggregates are known to be metastable, as at first they possess a large surface area to volume ratio and then undergo a relaxation towards a more stable configuration.<sup>36</sup> By observing these GO/rGO surfactant systems over time, it can be seen that this is indeed the case (see insets to (Fig. 6a–c), as the flocs eventually settle into a more condensed network at the bottom of their vessels (see also Supplementary Information); similar compaction over time of fractal aggregates has been observed recently in yttrium aluminium garnet systems also analysed by SANS.<sup>37</sup>

## Conclusions

In summary, we have shown that by incorporating a photosensitive surfactant molecule with a cationic head-group into aqueous carbon nanomaterial systems, it is possible to control the dispersion state of these materials using only light as a clean and low energy external stimulus. Using photoisomerisation to subtly shift the equilibrium between free and adsorbed surfactant, the carbon-based materials can be reversibly dispersed and flocculated. Crucially, by exploring a wide range of conditions including concentration and pH effects, it becomes clear that charge is not the only factor at play, and that surfactant adsorption occurs also via  $\pi$ -stacking and van der Waals type interactions. The photo-modulated flocculation of CNMs provides a facile means of recovering these materials from solution, enhancing opportunities for their application, processing and deployment in aqueous systems.

## Acknowledgements

We thank the Monash Centre for Atomically Thin Materials for providing funding that supported this project, and we acknowledge the support of the Bragg Institute, Australian Nuclear Science and Technology Organisation, in providing the neutron research facilities used in this work. We would also like to acknowledge the Monash Centre for Electron Microscopy for the use of their facilities.

## References

- 1 K. S. Novoselov, A. K Geim, S. V. Morozov, D. Jiang, Y. Zhang, S. V. Dubonos, I. V. Grigorieva and A. A. Firsov, *Science*, 2004, **306**, 666–669.
- 2 M. Lotya, P. J. King, U. Khan, S. De and J. N. Coleman, *ACS Nano*, 2010, **4**, 3155–3162.
- 3 D. Li, M. B. Muller, S. Gilje, R. B. Kaner and G. G. Wallace, *Nat. Nanotechnol.*, 2008, **3**, 101–105.
- 4 B. Konkena and S. Vasudevan, *J. Phys. Chem. Lett.*, 2012, **3**, 867–872.
- 5 F. Kim, L. J. Cote and J. Huang, *Adv. Mater.*, 2010, **22**, 1954–1958.
- 6 T. M. McCoy, M. J. Pottage and R. F. Tabor, *J. Phys. Chem. C*, 2014, **118**, 4529–4535.
- 7 G. Z. Kyzas, E. A. Deliyanni and K. A. Matis, *J. Chem. Technol. Biotechnol.*, 2014, **89**, 196–205.
- 8 T. M. McCoy, P. Brown, J. Eastoe and R. F. Tabor, *ACS Appl. Mater. Interfaces*, 2015, **7**, 2124–2133.
- 9 K. C. Kemp, H. Seema, M. Saleh, N. H. Le, K. Mahesh, V. Chandra and K. S. Kim, *Nanoscale*, 2013, **5**, 3149–3171.
- 10 A. Estévez-Torres, C. Crozatier, A. Diguët, T. Hara, H. Saito, K. Yoshikawa and D. Baigl, *Proc. Natl. Acad. Sci. U. S. A.*, 2009, **106**, 12219–12223.
- 11 A. Vesperinas, J. Eastoe, S. Jackson and P. Wyatt, *Chem. Commun.*, 2007, 3912–3914.
- 12 S. L. Gilat, S. H. Kawai and J.-M. Lehn, *Chem. Eur. J.*, 1995, **1**, 275–284.
- 13 A. S. Kumar, T. Ye, T. Takami, B.-C. Yu, A. K. Flatt, J. M. Tour and P. S. Weiss, *Nano Lett.*, 2008, **8**, 1644–1648.
- 14 S. Shinkai, K. Matsuo, A. Harada and O. J. Manabe, *Chem. Soc. Perkin Trans. 2*, 1982, 1261–1265.
- 15 X. Liu and N. L. Abbott, *J. Colloid Interface Sci.*, 2009, **339**, 1–18.

- 16 P. Brown, C. P. Butts and J. Eastoe, *Soft Matter*, 2013, **9**, 2365-2374.
- 17 M. Dubecky, R. Derian, L. Mitas and I. Stich, *J. Chem. Phys.*, 2010, **133**, 244301/1-5.
- 18 J. Eastoe and A. Vesperinas, *Soft Matter*, 2005, **1**, 338-347.
- 19 L. Vaisman, H. D. Wagner and G. Marom, *Adv. Colloid Interface Sci.*, 2006, **128**, 37-46.
- 20 S. Stankovich, D. A. Dikin, R. D. Piner, K. A. Kohlhaas, A. Kleinhammes, Y. Jia, Y. Wu, S. T. Nguyen and R. S. Ruoff, *Carbon*, 2007, **45**, 1558-1565.
- 21 S. Park, J. An, I. Jung, R. D. Piner, S. J. An, X. Li, A. Velamakanni and R. S. Ruoff, *Nano Lett.*, 2009, **9**, 1593-1597.
- 22 G. K. Ramesha, A. V. Kumara, H. B. Muralidhara and S. Sampath, *J. Colloid Interface Sci.*, 2011, **361**, 270-277.
- 23 E. Fischer, M. Frankel and R. Wolovsky, *J. Chem. Phys.*, 1995, **23**, 1367.
- 24 J. Griffiths, *Chem. Soc. Rev.*, 1972, **1**, 481-492.
- 25 E. Chevallier, A. Mamane, H. A. Stone, C. Tribet, F. Lequeux and C. Monteux, *Soft Matter*, 2011, **7**, 7866-7874.
- 26 H. M. D. Bandara and S. C. Burdette, *Chem. Soc. Rev.*, 2012, **41**, 1809-1825.
- 27 C. T. Lee Jr., K. A. Smith and T. A. Hatton, *Langmuir*, 2009, **25**, 13784-13794.
- 28 A.-L. Le Ny, C. T. Lee Jr., *J. Am. Chem. Soc.* 2006, **128**, 6400-6408.
- 29 L. M. Woods, Ş. C. Bădescu and T. L. Reinecke, *Phys. Rev. B*, 2007, **75**, 155415.
- 30 Y. Liu, J. Zhang, X. Chen, J. Zheng, G. Wang and G. Liang, *RSC Adv.*, 2014, **4**, 58036.
- 31 Y. Zhu, W. Cai, R. D. Piner, A. Velamakanni and R. S. Ruoff, *Appl. Phys. Lett.*, 2009, **95**, 103104.
- 32 I. K. Moon, J. Lee, R. S. Ruoff and H. Lee, *Nat. Commun.*, 2010, **1**, 73.
- 33 J. Yu, N. Groissord, C. E. Koning and J. Loos, *Carbon*, 2007, **45**, 618-623.
- 34 O. Matarredona, H. Rhoads, Z. Li, J. H. Harwell, L. Balzano and D. E. Resasco, *J. Phys. Chem. B*, 2003, **107**, 13357-13367.
- 35 W. W. Mullins and R. F. Sekerka, *J. Appl. Phys.*, 1963, **34**, 323-329.
- 36 R. Q. Hwang, J. Schröder, C. Günther and R. J. Behm, *Phys. Rev. Lett.*, 1991, **67**, 3279-3282.
- 37 J. Bahadur, S. Mazumder, D. Sen and S. J. Ramanathan, *Phys.: Condens. Matter*, 2010, **22**, 195107/7.